Analytical Force Calculation in Brushless-DC Motors II: Mathematical Details of the Alternative Approach

Ewgenij Starschich
University of Warwick
Coventry, CV4 7AL, UK
e.starschich@warwick.ac.uk

Annette Muetze
University of Warwick
Coventry, CV4 7AL, UK
a.muetze@warwick.ac.uk

Kay Hameyer
RWTH Aachen University
52056 Aachen, Germany
kay.hameyer@iem.rwth-aachen.de

***Abstract*—Expanding Part I of our contribution, this paper deals with the analytical calculation of the tangential forces in brushless dc machines, where we extend previously developed methods using conformal mapping and the Maxwell stress theory to enable a greater applicability of such methods. While Part I focuses on the explanation of the methodology itself, aiming to convey the overall picture and not to obscure the message with lengthy developments of formulae, this present Part II provides the detailed developments of the different expressions that are important for those to carry out further research in this area.**

***Index Terms*—Conformal mapping, brushless DC machine, design methodology, optimization.**

NOMENCLATURE

BLDCM	Brushless DC machine
EMF	Electromotive force
FEM	Finite element method
PM	PM
a	Transformation point in the conf. transf. $Z \rightarrow W$
A	Area
b	Transformation point in the conf. transf. $Z \rightarrow W$
B	Magnetic flux density
d_s	Slot depth
f	Force density
f_v	Volumic force density
F	Force
F_a	Armature force
F_c	Cogging force
g'	Air gap width in the Z-plane
H	Magnetic field strength
J	Current density
k	Coordinates in the K-plane
l_i	Effective machine length
p	Compressive stress tensor
R	Radius (machine geometry)
R_s	Stator inner surface radius
V	Volume
s	Coordinates in the S-plane
S^m	Maxwell stress tensor
t	Coordinates in the T-plane
w	Coordinates in the W-plane
z	Coordinates in the Z-plane
ε	Auxiliary parameter
$\lambda_{ks,m}$	Coordinate transformation factor for $K \rightarrow S$ (calculation of the PM field)
$\lambda_{ts,a}$	Coordinate transformation factor for $T \rightarrow S$ (calculation of the armature winding field)
μ	Permeability
μ_0	Permeability of vacuum, $\mu_0 = 4\,\pi 10^{-7}$ Vs/(Am)
μ_{fe}	Permeability of iron
μ_r	Relative permeability
σ	Tensile stress tensor
θ	Angle (machine geometry)
Indices	
1	Parameter on slot side no. 1
2	Parameter on slot side no. 2
a	Parameter related to the armature winding field
l	Parameter related to the tensile stress
m	Parameter related to the PM field
n	Component perpendicular to the material surface
q	Parameter related to the compressive stress
t	Component tangential to the material surface

I. INTRODUCTION

In this paper, continuing Part I of our contribution, we continue to focus on the analytical calculation of the tangential forces that generate the armature and the cogging torque in brushless dc machines (BLDCMs). This is motivated by the increasing complexity of electric drive systems which calls for the development of efficient design techniques for electric machines that still meet the desired degree of accuracy. While Part I focuses on the explanation of the methodology itself, aiming to convey the overall picture and not to obscure the message with lengthy developments of formulae, this present Part II provides the detailed derivations of the different newly developed expressions that are important for those to carry out further research in this area. Key aspects of the overall context that are required to develop those new expressions are reviewed in a concise manner so that not only Part I, but also Part II can be studied as a self-contained paper, with the same overall topic as Part I, but a different emphasis.

We have chosen BLDCMs as our application, because they can benefit even more than other machine types from an analytical technique that takes into account both the armature and the pulsating torque for fast optimization of the machine parameters and the control technique in one unified step. However, this should not obscure the fact that the presented technique can be expanded to be used in different machines and for the calculation of other (i.e. radial) forces.

Our new approach extends previously presented methods using conformal mapping to (i) avoid the singularity of the magnetic flux density at the tooth tip during the transformation and thereby overcome the limitations of this approach with respect to the calculation of the cogging and armature torques developed in electric machines, and (ii) calculate the forces

978-1-4244-4252-2/09/$25.00 ©2009 IEEE

at the slot sides so that the influence of the machine design parameters on the result is directly available.

To this aim, we use the Maxwell stress theory to calculate the forces at the interface of two materials with different permeabilities. While the Maxwell stress theory is frequently used to calculate the force on a rigid body placed in an electromagnetic field, very few results exist for the first method. The force on a rigid body method has the advantage that the contour can be freely selected. However, the vectorial components of the magnetic flux density along the contour have to be known and the relationship between the machine design parameters and the developed torque is not straightforward, since it is not obvious where the force physically occurs and therefore which part or parameter of the machine it is mostly influenced by. We therefore focus on the calculation of the forces on the interface of materials with different permeabilities, because of its suitability for analytical design and optimization techniques and the direct availability of the correlation between the machine geometrical parameters and the produced torque. This theory is discussed in detail in Sec. II.

Using this technique, the magnetic flux density at the slot sides needs to be known. Using available techniques to calculate the flux in slotted machines based on conformal transformations, a singularity occurs at the tooth tip, rendering the determination of the magnetic flux at this point impossible. Because these formulae are essential for the work presented in the following, they will be briefly reviewed in Sec. III. The singularity at the tooth tip significantly limits the calculation of the torque based on flux densities determined via conformal mapping, because of the crucial influence of the flux density in this area on the overall developed tangential forces.

In the new approach, we avoid the need to explicitly calculate the magnetic flux at the tooth tips by substituting the value of the magnetic flux density in the slotted machine by the magnetic field in the slotless machine and the corresponding transformation parameters. The new expressions for the armature and the cogging torque are developed in detail in Sec. IV, thereby complementing Part I of our contribution.

II. Discussion of the Maxwell Stress Theory

In the context of electric machines, the Maxwell stress theory is frequently used to calculate the developed torque(s) through computation of the force on a rigid body placed in an electromagnetic field. This easily obscures the fact that the Maxwell stress theory can also be used to calculate the forces at the interface of materials with different permeabilities. As a matter of fact, it has only rarely been discussed in the literature so far, with [1] and [2] being the two key references. In contrast to the rigid body method, this approach does not require the computation of the vectorial components of the magnetic flux density but only of the overall magnitude. Furthermore, the correlation between the machine's geometrical parameters and the produced torque is readily available. These benefits come at the expense that the integration path is given by the interface at which the force occurs and can hence not be freely selected, which clearly is an advantage of the rigid body method. Both methods are discussed in the following, with a special emphasis on the detailed derivation of the magnetic force at the interface of materials with different permeabilities.

A. Force on a rigid body placed in an electromagnetic field

The mutual forces between elements of charge are calculated via the assumption that a fictitious state of stress exists throughout the field, even in space free of matter, where the representation of magnetostatic stress components has no essential physical reality [3]. First, multiplying the first Maxwell equation in its form for stationary and quasi-static fields, $\nabla \times \vec{H} = \vec{J}$, vectorially by $\vec{B}$ and considering the material properties $\vec{B} = \mu_0 \mu_r \vec{H}$, with $\mu_r = 1$ in free space, one obtains

$$\frac{1}{\mu_0}\left(\nabla \times \vec{B}\right) \times \vec{B} = \vec{J} \times \vec{B}\,. \tag{1}$$

The right term of (1) describes the force per unit volume in a volume V containing moving charges and magnetic flux density. The total force on the given volume V is therefore

$$\vec{F}_m = \int_V \vec{J} \times \vec{B}\, dv\,. \tag{2}$$

In a rectangular coordinate system and assuming the magnetic flux density as divergence free, (1) can be written as

$$\frac{1}{\mu_0}\left(\nabla \times \vec{B}\right) \times \vec{B} + \frac{1}{\mu_0}\vec{B}\nabla \cdot \vec{B} = \operatorname{div} S^m \tag{3}$$

with the *Maxwell stress tensor* S^m

$$S^m = \begin{pmatrix} \frac{B_x^2}{\mu_0} - \frac{B^2}{2\mu_0} & \frac{B_x B_y}{\mu_0} & \frac{B_x B_z}{\mu_0} \\ \frac{B_y B_x}{\mu_0} & \frac{B_y^2}{\mu_0} - \frac{B^2}{2\mu_0} & \frac{B_y B_z}{\mu_0} \\ \frac{B_z B_x}{\mu_0} & \frac{B_z B_y}{\mu_0} & \frac{B_z^2}{\mu_0} - \frac{B^2}{2\mu_0} \end{pmatrix}. \tag{4}$$

For the complex steps of this reformulation, we refer to the literature (e.g. [3]). Next, one obtains

$$\int \operatorname{div} S^m dV = \vec{F}_m \quad \text{and} \quad \int S^m \vec{n}\, da = \vec{F}_m\,, \tag{5}$$

from (2) and (3) and using Gauss' Theorem, and the force density at the surface bounding the volume V

$$\vec{f}_m = \frac{d\vec{F}_m}{da} = S^m \vec{n}\,. \tag{6}$$

In a rectangular system, the product $S^m \vec{n}$ and hence the force density $\vec{f}_m$ can also be written as

$$S^m \vec{n} = \vec{f}_m = \frac{1}{\mu_0}\left(\vec{B} \cdot \vec{n}\right) \cdot \vec{B} - \frac{1}{2\mu_0} B^2 \cdot \vec{n}\,. \tag{7}$$

Using this approach, the boundary of the region can be freely selected. In the context of electric machines, the contour is frequently placed in the air gap [4] where it can be determined without any restriction. However, the required calculation of not only the absolute values of the magnetic flux along this contour, but also of its vectorial components increases the computational complexity significantly. Furthermore, the relationship between the machine design parameters and the developed torque is not straightforward, since it is not obvious where the force physically occurs and therefore which part or parameter of the machine it is mostly influenced by.

B. Force on the interface between materials with different permeabilities

The derivation of the forces between materials with different permeabilities is based on the assumption that a tensile stress σ exists inside a magnetic flux tube along the line of force trying to shorten the tube, and a compressive stress p at right angles to the line of force, trying to widen it [2]. Both σ and p depend on the material properties. (See also Sec. III-C of Part I of our contribution.) First, we review the development of the general expressions of the forces assuming these stresses are known [2]. Then, we derive the formulae taking into account the material assumptions of Helmholtz and Carter [1] explicitly, thereby extending the previous work.

1) General expression: Fig. 1 shows the magnetic flux vector at the interface between materials with different permeabilities. Assuming there is no surface charge at the interface, the well-known boundary conditions $H_{1t} = H_{2t}$ and $B_{1n} = B_{2n}$ hold true. Assuming the flux density $\vec{B}_1$ having an angle α_1 to the surface of area 1, the tensile and compressive forces of the magnetic flux density vector (Fig. 2(a)), are

$$dF_{1l} = \sigma \cdot dA \cdot \cos\alpha_1 \,, \tag{8}$$

$$dF_{1q} = p \cdot dA \cdot \sin\alpha_1 \,, \tag{9}$$

from which the resulting normal and tangential force components and the respective force densities are obtained:

$$\begin{aligned} dF_{1n} &= dF_{1l} \cdot \cos\alpha_1 - dF_{1q} \cdot \sin\alpha_1 \\ &= \sigma \cdot \cos^2\alpha_1 \cdot dA - p \cdot \sin^2\alpha_1 \cdot dA \,, \end{aligned} \tag{10}$$

$$\begin{aligned} dF_{1t} &= dF_{1l} \cdot \sin\alpha_1 + dF_{1q} \cdot \cos\alpha_1 \\ &= (\sigma + p) \cdot \cos\alpha_1 \cdot \sin\alpha_1 \cdot dA \,, \end{aligned} \tag{11}$$

$$f_{1n} = \frac{dF_{1n}}{dA} = \sigma \cdot \cos^2\alpha_1 - p \cdot \sin^2\alpha_1 \,, \tag{12}$$

$$f_{1t} = \frac{dF_{1t}}{dA} = (\sigma + p) \cdot \cos\alpha_1 \cdot \sin\alpha_1 \,. \tag{13}$$

The flux density $\vec{B}_2$ on side 2 also creates forces at the interface between the materials (Fig. 2(b)), which are in analogy to those on side 1 given as

$$f_{2n} = \frac{dF_{2n}}{dA} = -\left(\sigma \cdot \cos^2\alpha_2 - p \cdot \sin^2\alpha_2\right) \,, \tag{14}$$

$$f_{2t} = \frac{dF_{2t}}{dA} = (\sigma + p) \cdot \cos\alpha_2 \cdot \sin\alpha_2 \,. \tag{15}$$

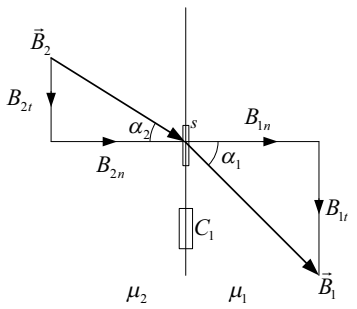

Fig. 1. Magnetic field vectors at the interface of two materials with different magnetic permeabilities.

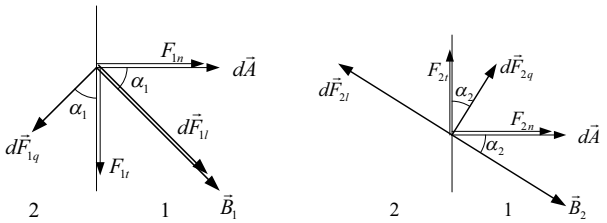

(a) Area 1. (b) Area 2.

Fig. 2. Tensile and compressive components of the force vectors in the two areas.

The expressions for the resulting normal and tangential force densities are obtained by superposition,

$$f_n = f_{1n} + f_{2n} \quad \text{and} \quad f_t = f_{1t} + f_{2t} \,. \tag{16}$$

2) Helmholtz' material assumptions: The tensile and compressive forces σ and p, derived from Helmholtz' material assumptions, are [1]

$$\sigma = p = \frac{1}{2}BH \,, \tag{17}$$

from which (13) becomes

$$\begin{aligned} f_{1n} &= \frac{1}{2}B_1H_1\cos^2\alpha_1 - \frac{1}{2}B_1H_1\sin^2\alpha_1 \\ &= \frac{1}{2\mu_1} \cdot \left(B_{1n}^2 - B_{1t}^2\right) \,. \end{aligned} \tag{18}$$

With the normal force density in area 2 derived accordingly

$$f_{2n} = -\frac{1}{2\mu_2} \cdot \left(B_{2n}^2 - B_{2t}^2\right) \,, \tag{19}$$

the total normal force component $f_n = f_{1n} + f_{2n}$ becomes:

$$f_n = \frac{1}{2} \cdot \left(\frac{1}{\mu_1} - \frac{1}{\mu_2}\right)\left(B_{1n}^2 + \frac{\mu_2}{\mu_1}B_{1t}^2\right) \,. \tag{20}$$

$$\begin{aligned} f_{1t} &= \left(\frac{1}{2}B_1H_1 + \frac{1}{2}B_1H_1\right) \cdot \cos\alpha_1 \cdot \sin\alpha_1 \\ &= B_{1n}H_{1t} = \frac{1}{\mu_1}B_{1n}B_{1t} \,, \end{aligned} \tag{21}$$

$$f_{2t} = -\frac{1}{\mu_1}B_{2n}B_{2t} \,, \tag{22}$$

$$f_t = f_{1t} + f_{2t} = \frac{1}{\mu_1}B_{1n}B_{1t} - \frac{1}{\mu_1}B_{1n}B_{1t} = 0 \,. \tag{23}$$

With Helmholtz' material assumptions, the total force has only a normal force component. *The direct implication from the Helmholtz σ and p definitions for electric machine applications is that the torque can only be generated at the tooth sides. The field component at the tooth head causes radial forces and does not have a tangential force component.*

In the context discussed here, only the interfaces between iron and materials with $\mu \ll \mu_{fe}$ are of interest. Furthermore, without loss of generality, we simplify $\mu = \mu_0$ throughout the whole slot. With $\mu_2 = \mu_r\mu_0$ and therefore $\mu_1 = \mu_0$, (16 a) becomes

$$f_n = \frac{1}{2} \cdot \left(\frac{1}{\mu_0} - \frac{1}{\mu_r\mu_0}\right)\left(B_{1n}^2 + \mu_r B_{1t}^2\right) \,. \tag{24}$$

Assuming furthermore $\mu_r \to \infty$, it is $B_t \to 0$, and the force density at the interface is finally

$$f_n = \frac{1}{2\mu_0} B^2 \ . \tag{25}$$

3) Carter's material assumptions: Carter made different material assumptions, resulting in [1]

$$\sigma \ = \ \frac{1}{2\mu_0} B^2 \ \text{ and } \ p = \frac{\mu_0}{2} H^2 \tag{26}$$

for the tensile and compressive stresses, from which the normal and tangential force densities at the interface between two materials with $\mu_1 = \mu_0$ and $\mu_2 = \mu_r \mu_0$,

$$f_n \ = \ \frac{1}{2} \frac{B_{1n}^2 - H_{1t}^2}{\mu_0} - \frac{1}{2} \left(\frac{B_{2n}^2}{\mu_0} - \mu_0 H_{2t}^2 \right) = 0 \ , \tag{27}$$

$$f_t \ = \ - \frac{(\mu_r - 1)^2}{2\mu_r} \cdot H_{1n} \cdot H_{1t} \tag{28}$$

are obtained.

Using Carter's material assumptions, only a tangential force exists at the interface between materials with different permeabilites. However, as the magnetic field becomes perpendicular to the surface for $\mu_r \to \infty$, the tangential force component (28) would also diminish for this "ideal" case.

Unlike with Helmholtz' assumptions, Carter's material assumptions and therefrom derived stresses can also cause forces within the material. The volumic iron force density inside the material is given by

$$f_v = \vec{J} \times \vec{B} + \mu_0 \left(\frac{\mu_r^2 - 1}{2} \right) \nabla \left(\frac{1}{2} H^2 \right) \ , \tag{29}$$

where the term $\vec{J} \times \vec{B}$ expresses a force density due to currents within the iron, which–neglecting eddy currents–are usually not present. The second term gives the force density which is directed towards the regions with a higher flux density.

C. Conclusions on the material assumptions

The two different definitions of σ and p lead to significantly different results of the developed forces which (for μ_1 and μ_2 as defined above) can be summarized as follows:

1) Helmholtz' material assumptions give surface forces normal to the surface, but no volumic forces. The surface forces do not depend on the orientation of the flux but only on its absolute magnitude, and are directed from the material with the higher to the one with the lower permeability.
2) Carter's material assumptions give both surface and volumic forces. The surface forces are tangential to the surface and are zero when the magnetic field is tangential or perpendicular to the surface. The volumic forces inside the material tend to force each element towards the parts with the higher magnetic flux density.

For accurate analysis of the forces acting inside a machine, both assumptions should be examined. However, no literature is known to the authors in which Carter's material assumptions are used and the machine torque is analyzed based on the field calculated inside the iron. *In the further analysis, Helmholtz' material assumptions will be used* because the resulting analysis is more concordant with the common techniques of machine analysis and the calculation of the field inside the iron of the machine is more complex than the one at the material interfaces.

D. Application to electric machine design

1) Implications and approximations: For electric machines, Helmholtz' material assumptions imply that the torque can only be generated at the tooth sides. The field component at the tooth head causes radial forces and does not have a tangential component. Furthermore, we have $\mu \ll \mu_{fe}$ in the slot. Without loss of generality of the methodology presented, we approximate $\mu = \mu_1 \approx \mu_0$ throughout the slot and refer to the results developed in Sec. II-B2: with the permeability of the core $\mu_2 = \mu_r \mu_0$ (24) applies, what, assuming furthermore $\mu_r \to \infty$ and hence $B_t \to 0$, further simplifies to (25). As long as these assumptions hold true (within the desired degree of accuracy), *only the absolute value of the flux distribution along the slot sides is required for the calculation of the cogging and armature force*, which is a huge advantage over the force on a rigid body/contour in the air gap method.

2) Cogging force: For a given rotor position, using (25), the total force acting on one slot side and caused by the fields generated by the permanent magnets (PMs) is

$$F_c = \frac{1}{2\mu_0} \cdot l_i \cdot \int_{R_s}^{R_s + d_s} B_m^2 \ dR \ , \tag{30}$$

with the effective stator length l_i, the inner stator radius R_s, the slot depth d_s, and the index m to indicate that the magnetic field is generated by the PMs. If a slot is fully covered by a magnet, the forces on the two slot sides cancel each other. If a given slot is only partially covered by a magnet, a resultant force normal to the slot surface and hence tangential to the machine radius occurs. These forces cause the cogging torque, which therefore can be computed from the sum of all the forces F_c that are acting on the individual slot sides, and considering the radius the force is active at.

3) Armature force: The desired tangential force that generates the armature torque is caused by the field generated by the armature winding, which strengthens the field generated by the PMs on the one and weakens it on the other side of the slot the winding is placed in. Again, using (25), the resulting force in the slot is derived in analogy to (30),

$$\begin{aligned} F_a \ &= \ \frac{1}{2\mu_0} \cdot l_i \cdot \int_{R_s}^{R_s + d_s} \Big(\Big| \vec{B}_m(R, \theta_2) - \vec{B}_a(R, \theta_2) \Big|^2 \\ &- \ \Big| \vec{B}_m(R, \theta_1) + \vec{B}_a(R, \theta_1) \Big|^2 \Big) \, dR \ , \end{aligned} \tag{31}$$

where θ_1 and θ_2 are the angles of the two slot sides respectively. For straightforwardness, we only consider slots fully covered by a magnet and exploit the symmetry, i.e. $|\vec{B}(R, \theta_1)| = |\vec{B}(R, \theta_2)| = |\vec{B}(R)|$, both for B_m and B_a,

and finally obtain

$$F_a = -\frac{2}{\mu_0} \cdot l_i \cdot \int_{R_s}^{R_s+d_s} \left|\vec{B}_m(R)\right| \left|\vec{B}_a(R)\right| \, dR \, . \qquad (32)$$

III. Summary of the Conformal Transformations Used

For our new approach to compute the cogging and armature torque, we apply the conformal transformation used in [5] for the calculation of the magnetic field generated by the armature winding and the one presented in [6] (which is based on [7], [8], and [5]) for the computation of the field generated by the PMs, respectively. In both cases, the air gap field is calculated for a slotless machine and then the slotting is taken into account through multiplication with a complex permeance.

This approach includes the following simplifications: (i) $\mu_{fe} \rightarrow \infty$, (ii) no change of the field distribution in axial direction, (iii) rectangular, and (iv) infinitely deep slots, and the–in line with (ii)–radially magnetized PMs are (v) assumed to have a linear second-quadrant demagnetization characteristic, (vi) are modeled by surface currents at the magnet flanks, neglecting any volume currents inside the PMs [9].

For the magnetic field generated by the PMs, four conformal transformations are required, transforming the geometry between the planes S (slotted machine), Z, W, T and K (slotless machine) [6]. If a slot is fully covered by a magnet, the magnetic field in the K-plane is constant. Otherwise, if a slot is not fully covered by a magnet, a transition area between zero field and maximum field exists. The width of the transition area depends on the geometrical parameters of the machine and notably on the dimensions of the magnet. An analytic expression for the magnetic field in the slotless machine generated by the PMs, B_{km}, has been derived in [7], which is also used the work presented here.

For the armature field, only three conformal transformations are required: $S \rightarrow Z$, $Z \rightarrow W$, and $W \rightarrow T$ [5]. Since the line of symmetry in the middle of the slot can be exploited only half of the slot needs to be analyzed. Note that in both cases, an analytical transformation $Z \rightarrow W$ is not possible and numerical methods have to be applied. For further details on the individual steps, we refer to Part I of our contribution as well as to the cited literature.

Using these conformal transformations, the fields generated by the PMs and by the armature winding in the slotted machine, B_{sm} and B_{sa}, can be obtained from those computed for the slotless machines, B_{km} and B_{ta}, by

$$B_{sm} = B_{km} \cdot \left(\frac{\partial k_m}{\partial s_m}\right)^* , \qquad (33)$$

$$B_{sa} = B_{ta} \cdot \left(\frac{\partial t_a}{\partial s_a}\right)^* , \qquad (34)$$

from which

$$B_{sm} = \lambda^*_{ks,m} \cdot B_{km} \, , \qquad (35)$$

$$B_{sa} = \lambda^*_{ts,a} \cdot B_{ta} \, , \qquad (36)$$

with the complex permeances

$$\lambda_{ks,m} = \frac{k_m}{s_m} \cdot \frac{w_m - 1}{\sqrt{w_m - a_m}\sqrt{w_m - b_m}} = \lambda_m \, , \qquad (37)$$

$$\lambda_{ts,a} = j \cdot \frac{1}{g'} \frac{\sqrt{w_a - a_a}}{\sqrt{w_a + 1}} \cdot \frac{1}{s_a} = \lambda_a \qquad (38)$$

can be obtained. Here, '*' denotes the complex conjugate, g' the width of the air gap in the Z-plane, k, w, and s are the coordinates in the K-, W-, and S-plane respectively, and $a_m = 1/b_m$ and a_a are transformation points for the transformation $Z \rightarrow W$. For the derivations of the magnetic field distributions in a slotless PM machine, B_{km} and B_{ta}, as well as of the complex permeances λ_m and λ_a, we refer to the literature (i.e. [5]–[8]). The full expressions of $\lambda_{ks,m} = \frac{\partial k_m}{\partial s_m}$ and $\lambda_{ts,a} = \frac{\partial t_a}{\partial s_a}$, i.e. the individual partial derivatives contributing to these terms, are required to understand the detailed derivations of the new expressions to compute the forces that cause the cogging and armature torque in BLDCMs. They are therefore given in the Appendix.

It is important to note that (37) does not have a solution for $w_m = a_m = b_m$ which correspond to the tooth tips of the slotted, "real" machine in the S-plane.

IV. The New Force and Torque Calculation Method

A. Introduction

In Part I of our contribution we have shown that the majority of the field generated by the PMs strongly decreases with the distance from the tooth tip, and that therefore the singularity in (37) significantly limits the use of this method as such to compute the armature and cogging torque generated in the machine. This has been highlighted by the computation of the cogging torque in an example machine with $d_s = 10\,\text{mm}$ deep slots. Here, the field was computed up to distance ε from the tooth tips. The very small difference of $0.003\,\text{mm}$ ($\varepsilon_1 = 0.01\,\text{mm}$ versus $\varepsilon_2 = 0.007\,\text{mm}$) resulted in computed torque values differing by more than a factor of 2.5!

In the new approach, we avoid the need to explicitly calculate the magnetic flux at the tooth tips by substituting the values of the magnetic flux density in the slotted machine $B_{sm} = B_m$ and $B_{ta} = B_a$ in the expressions for F_c and F_a by the magnetic fields in the slotless machine B_{km} and B_{ta} and the corresponding transformation parameters λ_m and λ_a. Thereby, the forces F_c and F_a are calculated in one step and no singularities occur any more in the expression, as will become clear in the following.

B. Cogging force

In order to account for the different planes considered in the approach, the general expression for the force resulting from the field generated by the PMs (30) is rewritten, considering that the magnetic field generated by the PMs, B_m, is the field in the slotted machine in the S-plane,

$$F_c = \frac{1}{2\mu_0} \cdot l_i \cdot \int_{R_s}^{R_s+d_s} B_m^2 \, ds \, . \qquad (39)$$

Then, the integration limits are adjusted to account for the infinite slot depth required for the conformal mapping,

$$F_c = \frac{1}{2\mu_0} \cdot l_i \cdot \int_{R_s}^{\infty} B_m^2 \, ds \; . \tag{40}$$

The influence of this adjustment on the accuracy of the results is negligible, because of the strong decrease of the magnetic flux density with the slot depth. Next, the magnetic flux density is replaced using (35),

$$F_c = \frac{1}{2\mu_0} \cdot l_i \cdot \int_{R_s}^{\infty} \left| \lambda^*_{ks,m} \cdot B_{km}(s) \right|^2 \, ds \; . \tag{41}$$

The force calculation with (41) is not directly possible because $B_{km}(s)$ is not available. From [7] the magnetic flux density in a slotless machine $B_{km}(k)$ is given. Therefore, the integration parameters and limits have to be adjusted. For this purpose we do not replace the complex permeance λ^*_{ks} directly by its expression (37) but by the corresponding derivation $\frac{\partial k_m}{\partial s_m}$, see (33),

$$\begin{aligned} F_c &= \frac{1}{2\mu_0} \cdot l_i \cdot \int_{R_s}^{\infty} |B_{km}(s_m)|^2 \cdot \left| \frac{\partial k_m}{\partial s_m} \right|^2 ds \\ &= \frac{1}{2\mu_0} \cdot l_i \cdot \int_{R_s}^{\infty} |B_{km}(s_m)|^2 \\ &\qquad \cdot \left| \frac{\partial k_m}{\partial t_m} \frac{\partial t_m}{\partial w_m} \frac{\partial w_m}{\partial z_m} \frac{\partial z_m}{\partial s_m} \right|^2 ds \; . \end{aligned} \tag{42}$$

Since the two slot sides are transformed to different points in the K-plane, they also have different new integration limits. In the following, we develop the new expression for the force at one slot side, F_{c1}, at length, the one for the second slot side, F_{c2}, follows accordingly.

In the first step, we transform the integral from the S- into the Z-plane by canceling the terms $\frac{1}{\partial s_m}$ and ds and adjusting the integration limits (logarithmic transformation).

$$\begin{aligned} F_{c1} &= \frac{1}{2\mu_0} \cdot l_i \cdot \int_{\log R_s + j\theta_1}^{\infty + j\theta_1} |B_{km}(z_m)|^2 \\ &\qquad \cdot \left| \frac{\partial k_m}{\partial t_m} \frac{\partial t_m}{\partial w_m} \frac{\partial w_m}{\partial z_m} \right|^2 \left| \frac{\partial z_m}{\partial s_m} \right| dz_m \end{aligned} \tag{43}$$

$$\begin{aligned} &= \frac{1}{2\mu_0} \cdot l_i \cdot \int_{\log R_s + j\theta_1}^{\infty + j\theta_1} |B_{km}(z_m)|^2 \\ &\qquad \cdot \left| \frac{\partial k_m}{\partial t_m} \frac{\partial t_m}{\partial w_m} \frac{\partial w_m}{\partial z_m} \right|^2 \left| \frac{1}{e^{z_m}} \right| dz_m \\ &= \frac{1}{2\mu_0} \cdot l_i \cdot \frac{1}{R_s} \cdot \int_{\log R_s + j\theta_1}^{\infty + j\theta_1} |B_{km}(z_m)|^2 \\ &\qquad \cdot \left| \frac{\partial k_m}{\partial t_m} \frac{\partial t_m}{\partial w_m} \frac{\partial w_m}{\partial z_m} \right|^2 dz_m \; . \end{aligned} \tag{44}$$

In the next step, the integral is transformed from the Z- into the W-plane in analogy to the previous transformation, (canceling $\frac{1}{\partial z_m}$ and dz_m and adjusting the integration limits; Schwarz-Christoffel transformation).

$$\begin{aligned} F_{c1} &= \frac{1}{2\mu_0} \cdot l_i \cdot \frac{1}{R_s} \cdot \int_{a_m}^{1} |B_{km}(w_m)|^2 \\ &\qquad \cdot \left| \frac{\partial k_m}{\partial t} \frac{\partial t}{\partial w} \right|^2 \left| \frac{\partial w_m}{\partial z_m} \right| dw_m \end{aligned} \tag{45}$$

$$\begin{aligned} &= \frac{1}{2\mu_0} \cdot l_i \cdot \frac{1}{R_s} \cdot \int_{a_m}^{1} |B_{km}(w_m)|^2 \\ &\qquad \cdot \left| k_m \cdot j \cdot \frac{g'}{\pi} \cdot \frac{1}{w} \right|^2 \\ &\qquad \cdot \left| -j \cdot \frac{\pi}{g'} \cdot \frac{(w_m - 1) \cdot w_m}{\sqrt{w_m - a_m} \cdot \sqrt{w_m - b_m}} \right| dw \\ &= \frac{1}{2\mu_0} \cdot l_i \cdot \frac{1}{R_s} \cdot \frac{g'}{\pi} \cdot \int_{a_m}^{1} |B_{km}(w)|^2 \\ &\qquad \cdot \left| R_s \cdot e^{j \cdot \left(\frac{g'}{\pi} \ln w_m + \frac{\theta_s}{2} \right)} \right|^2 \\ &\qquad \cdot \left| \frac{w_m - 1}{w_m \cdot \sqrt{w_m - a_m} \cdot \sqrt{w_m - b_m}} \right| dw \end{aligned} \tag{46}$$

$$\begin{aligned} &= \frac{1}{2\mu_0} \cdot l_i \cdot R_s \cdot \frac{g'}{\pi} \cdot \int_{a_m}^{1} |B_{km}(w_m)|^2 \\ &\qquad \cdot \left| \frac{w_m - 1}{w_m \cdot \sqrt{w_m - a_m} \cdot \sqrt{w_m - b_m}} \right| dw \; . \end{aligned} \tag{47}$$

Because of the conformal transformation the value of w_m is limited to $0 \leq a_m \leq w_m \leq 1$. We can therefore eliminate the absolute value bars and obtain the final expression for the force acting on the first side of the slot,

$$\begin{aligned} F_{c1} &= \frac{1}{2\mu_0} \cdot l_i \cdot R_s \cdot \frac{g'_m}{\pi} \cdot \int_{a_m}^{1} |B_{km}(w_m)|^2 \\ &\qquad \cdot \frac{1 - w_m}{w_m \cdot \sqrt{w_m - a_m} \cdot \sqrt{b_m - w_m}} \, dw_m \; . \end{aligned} \tag{48}$$

The force acting on the second side of the slot can be derived accordingly and is

$$\begin{aligned} F_{c2} &= \frac{1}{2\mu_0} \cdot l_i \cdot R_s \cdot \frac{g'_m}{\pi} \cdot \int_{1}^{b_m} |B_{km}(w_m)|^2 \\ &\qquad \cdot \frac{1 - w_m}{w_m \cdot \sqrt{w_m - a_m} \cdot \sqrt{b_m - w_m}} \, dw_m \; . \end{aligned} \tag{49}$$

The total contribution of one slot towards the force generating the cogging torque is

$$F_{c,slot} = F_{c1} + F_{c2} \; . \tag{50}$$

Note that only slots which are not fully covered by a PM magnet have $F_{c,slot} \neq 0$. The total cogging force can be

computed from (50) considering all slots of the machine which are not fully covered by a PM.

In Part I of our contribution we have shown results confirming that *the new approach to compute the cogging torque based on the magnetic field in the slotless machine and using a single expression is correct*. Because of a displacement of the angular position the maximum of the torque occurs at when the field in the slotless machine, B_{km} from [7], is obtained analytically instead of numerically, we concluded that further work to develop improved methods to calculate this field analytically would be preferable. However, *considering the sensitivity of numerical results for the cogging torque towards the simulation parameters and the related and required high computational effort, the results of the analytical calculation can be considered as acceptable.*

C. Armature force

The new expression to calculate the armature force is developed in analogy to the one to compute the cogging torque discussed in the previous paragraph: first, in order to account for the different planes considered in the approach, the general expression for the force resulting from the field generated by the PMs (32) is rewritten, considering that the magnetic fields generated by the PMs and by the armature winding B_m and B_a are those of the slotted machine in the S-plane, and adjusting the integration boundaries to account for the infinite slot depth required for the conformal mapping,

$$F_a = -\frac{2}{\mu_0} \cdot l_i \cdot \int_{R_s}^{\infty} \left|\vec{B}_{sm}(R)\right| \left|\vec{B}_{sa}(R)\right| \, dR \, . \tag{51}$$

Next, the magnetic flux densities are replaced using (35) and (36),

$$F_a = -\frac{2}{\mu_0} \cdot l_i \cdot \int_{Rs}^{\infty} \left|\lambda^*_{ks,m} \cdot B_{km}\right| \left|\lambda^*_{ts,a} \cdot B_{ta}\right| \, ds \, . \tag{52}$$

The armature winding field in the T-plane does not depend on the radius. Assuming that the slot is completely covered by the magnet and that the flux in the K-plane is therefore constant, equation (52) becomes

$$F_a = -\frac{2}{\mu_0} \cdot l_i \cdot |B_{km}| \, |B_{ta}| \cdot \int_{Rs}^{\infty} \left|\lambda^*_{ks,m}\right| \left|\lambda^*_{ts,a}\right| \, ds \, . \tag{53}$$

Again, as in the case of the cogging torque, we do not replace the complex permeances $\lambda^*_{ks,m}$ and $\lambda^*_{ts,a}$ directly by their expressions (37) and (38) but by the corresponding derivations $\frac{\partial k_m}{\partial s_m}$ and $\frac{\partial t_a}{\partial s_a}$ (expanded), in order to adjust the integration parameters and limits, see (33), (34), and the Appendix,

$$\begin{aligned} F_a &= -\frac{2}{\mu_0} \cdot l_i \cdot |B_{km}| \, |B_{ta}| \cdot \int_{R_s}^{\infty} \left|\frac{\partial k_m}{\partial t_m} \frac{\partial t_m}{\partial w_m} \frac{\partial w_m}{\partial z_m} \frac{\partial z_m}{\partial s_m}\right| \\ &\quad \cdot \left|\frac{\partial t_a}{\partial w_a} \frac{\partial w_a}{\partial z_a} \frac{\partial z_a}{\partial s_a}\right| \, ds \, . \end{aligned} \tag{54}$$

It is obvious that the coordinates in the S-plane for the computation of the magnetic fields generated by the PMs and by the armature winding are the same, $s_a = s_m = s$, since the same machine model is used for both cases. As in the previous case, we transform the integral from the S- into the Z-plane by canceling the terms $\frac{1}{\partial s_m}$ and ds and adjusting the integration limits (logarithmic transformation),

$$\begin{aligned} F_a &= -\frac{2}{\mu_0} \cdot l_i \cdot |B_{km}| \, |B_{ta}| \cdot \int_{\log R_s + j\theta_1}^{\infty + j\theta_1} \left|\frac{\partial k_m}{\partial t_m} \frac{\partial t_m}{\partial w_m} \frac{\partial w_m}{\partial z_m}\right| \\ &\quad \cdot \left|\frac{\partial t_a}{\partial w_a} \frac{\partial w_a}{\partial z_a} \frac{1}{e^{z_a}}\right| \, dz_m \end{aligned} \tag{55}$$

$$\begin{aligned} &= -\frac{2}{\mu_0} \cdot l_i \cdot |B_{km}| \, |B_{ta}| \cdot \frac{1}{R_s} \\ &\quad \cdot \int_{\log R_s + j\theta_1}^{\infty + j\theta_1} \left|\frac{\partial k_m}{\partial t_m} \frac{\partial t_m}{\partial w_m} \frac{\partial w_m}{\partial z_m}\right| \left|\frac{\partial t_a}{\partial w_a} \frac{\partial w_a}{\partial z_a}\right| \, dz_m \, . \end{aligned} \tag{56}$$

with $\left|\frac{\partial z_a}{\partial s_a}\right| = \left|\frac{1}{e^{z_a}}\right| \approx \frac{1}{R_s}$ (neglecting the slot depth when compared to the stator radius).

By changing the integration variables from the Z- to the W-plane coordinates and selecting the PM variable w_m as the new integration variable it is now necessary to determine the armature winding W-plane variable w_a as a function of the PM W-plane variable w_m. Because of the multiple transformations between different planes used in the conformal mapping, this step requires the determination of w_a as a function of z_a. However, as explained in Part I of our contribution (Sec. V-C), the transformation $Z \rightarrow W$ cannot be solved analytically and has to be solved numerically. To this aim, the solution of the transformation points $Z \rightarrow W$ is obtained numerically and the given points are interpolated, e.g. using the *MATHEMATICA* function *Interpolate* [10]. This numerical determination is more complex than the one used to calculate the flux density only. However, *this new approach bypasses the singularity problem at the tooth tip, so that the force can be calculated without any restrictions.*

In the last step, the integral is transformed from the Z- into the W-plane. With $g'_m = g'_a = g'$, as well as $\left|e^{j \cdot \left(\frac{g'}{\pi} \ln w + \frac{\theta_s}{2}\right)}\right| = 1$ for all g', w, and θ_s, the final expression of the armature force is obtained, (57),

$$\begin{aligned} F_a = &- \frac{2}{\mu_0} \cdot l_i \cdot |B_{km}| \, |B_{ta}| \cdot \frac{1}{R_s} \cdot \int_{a_m}^{1} \left|k \cdot j \cdot \frac{g'}{\pi} \cdot \frac{1}{w_m}\right| \\ &\cdot \left|\frac{1}{\pi} \frac{1}{w_a(w_m)} \cdot j \frac{\pi}{g'} \frac{w_a(w_m) \cdot \sqrt{w_a(w_m) - a_a}}{\sqrt{w_a(w_m) + 1}}\right| \\ &\qquad\qquad dw_m \end{aligned}$$

$$\begin{aligned} = &- \frac{2}{\mu_0 \pi} \cdot l_i \cdot |B_{km}| \, |B_{ta}| \cdot \frac{1}{R_s} \\ &\cdot \int_{a_m}^{1} \left|R_s \cdot e^{j \cdot \left(\frac{g'}{\pi} \ln w + \frac{\theta_s}{2}\right)} \cdot \frac{1}{w_m}\right| \\ &\qquad \left|\frac{\sqrt{w_a(w_m) - a_a}}{\sqrt{w_a(w_m) + 1}}\right| \, dw_m \end{aligned}$$

$$= \quad - \quad \frac{2}{\mu_0 \pi} \cdot l_i \cdot |B_{km}| \, |B_{ta}| \cdot \int_{a_m}^{1} \frac{1}{w_m} \left| \frac{\sqrt{w_a\,(w_m) - a_a}}{\sqrt{w_a\,(w_m) + 1}} \right| dw_m \ . \qquad (57)$$

Similar to the case of the cogging torque, we have shown results confirming that *this new approach to compute the armature torque is justified* in Part I of our contribution. As a matter of fact, for the example case machine, the difference between the analytical and the numerical solutions was *smaller than* 1%*, which is an excellent result*. While it is likely that such accuracy will not be obtained for other machine configurations, *the results prove that the armature force calculation assumptions and the implementation of the conformal mapping into the calculation of the force are correct and that they generally can be used for the force calculation*.

V. Conclusions

This paper reports on the technical details of a comprehensive analysis of the use of the Maxwell stress theory applied to calculate the forces at the interface of two materials with different permeabilities (as opposed to the forces on a rigid body placed in an electromagnetic field) and thereby to compute the armature and cogging torque in BLDCMs. In contrast to Part I of our contribution, where emphasis is laid on the methodology, this present Part II provides the detailed developments of the different expressions that are important for those to carry out further research in this area. First, we develop the formulae to compute the forces on the interface between materials with different permeabilities, taking the material properties explicitly into account. The expressions resulting from Helmholtz' material assumptions are then used to develop the expressions to calculate the cogging and armature forces that eventually cause the cogging and armature torque of an electric machine. In these computations, we avoid the need to explicitly calculate the magnetic flux at the tooth tips, as it occurs when the magnetic flux on the slot sides is directly computed using conformal mapping. Further work should include the development of improved methods to calculate the flux at the permanent magnet edges. Furthermore, the developed techniques should be applied to and analyzed for different machines with different geometries.

Appendix: Individual Complex Permeances of the Conformal Transformations

A. Field generated by the PMs (based on [6])

The partial derivative $\frac{\partial k_m}{\partial s_m}$ is not directly given but can be derived, considering the four transformations involved, $S \rightarrow Z \rightarrow W \rightarrow T \rightarrow K$,

$$\frac{\partial k_m}{\partial s_m} = \frac{\partial k_m}{\partial t_m} \frac{\partial t_m}{\partial w_m} \frac{\partial w_m}{\partial z_m} \frac{\partial z_m}{\partial s_m} \ , \qquad (58)$$

with the partial derivatives defined by the differential equation of the conformal transformations between the respective planes. These are:

$$\frac{\partial k_m}{\partial t_m} = e^{t_m} = e^{\ln k_m} = k_m \ , \qquad (59)$$

$$\frac{\partial t_m}{\partial w_m} = j \cdot \frac{g'}{\pi} \frac{1}{w} \ , \qquad (60)$$

$$\frac{\partial w_m}{\partial z_m} = -j \cdot \frac{\pi}{g'} \frac{w_m \cdot (w_m - 1)}{\sqrt{w_m - a_m}\sqrt{w_m - b_m}} \ , \qquad (61)$$

$$\frac{\partial z_m}{\partial s_m} = \frac{1}{s_m} = \frac{1}{e^{z_m}} \ . \qquad (62)$$

B. Field generated by the armature winding (based on [5])

As in the case of the field generated by the PMs, the partial derivative $\frac{\partial t_a}{\partial s_a}$ is not directly given but can be derived, considering the three transformations involved, $S \rightarrow Z \rightarrow W \rightarrow T$,

$$\frac{\partial t_a}{\partial s} = \frac{\partial t_a}{\partial w_a} \frac{\partial w_a}{\partial z_a} \frac{\partial z_a}{\partial s} \ . \qquad (63)$$

with the partial derivatives defined by the differential equation of the conformal transformations between the respective planes. These are:

$$\frac{\partial t_a}{\partial w_a} = \frac{1}{\pi} \frac{1}{w_a} \ , \qquad (64)$$

$$\frac{\partial w_a}{\partial z_a} = j \cdot \frac{\pi}{g'} \frac{w_a \cdot \sqrt{w_a - a_a}}{\sqrt{w_a + 1}} \ , \qquad (65)$$

$$\frac{\partial z_a}{\partial s_a} = \frac{1}{s_a} = \frac{1}{e^{z_a}} \ . \qquad (66)$$

References

[1] G.W. Carter, *The electromagnetic field in its engineering aspects*, Longman Group Limited, London, 1967.

[2] K. Vogt and G. Müller, *Berechnung rotierender elektrischer Maschinen*, VEB Verlag Technik Berlin, 1974.

[3] J.A. Stratton, *Electromagnetic theory*, McGraw-Hill, New York, London, 1941.

[4] W.R. Canders, "Grundlagen der Elektrischen Energietechnik-Elektrische Energieumformung," IMAB TU Braunschweig, Technical Report, 2007.

[5] K.J. Binns, P.J. Lawrenson, and C.W. Trowbridge, *The analytical and numerical solution of electric and magnetic fields*, John Wiley & Sons, Chichester, 1992.

[6] D. Zarko, D. Ban, and T.A. Lipo, "Analytical calculation of magnetic field distribution in the slotted air gap of a surface permanent-magnet motor using complex relative air-gap permeance," *IEEE Tr. Magn.*, vol. 42, no. 7, pp. 1828–1837, Jul 2006.

[7] Z.Q. Zhu and D. Howe, "Instantaneous magnetic field distribution in brushless permanent magnet DC motors I: Open-circuit field," *IEEE Tr. Magn.*, vol. 29, no. 1, pp. 124–135, Jan 1993.

[8] Z.Q. Zhu and D. Howe, "Instantaneous magnetic field distribution in brushless permanent magnet DC motors III: Effect of stator slotting," *IEEE Tr. Magn.*, vol. 29, no. 1, pp. 143–151, Jan 1993.

[9] N. Boules, "Prediction of No-Load Flux Density Distribution in Permanent Magnet Machines," *IEEE Tr. Ind. Appl.*, vol. IA-21, no. 3, pp. 633–643, May 1985.

[10] Mathematica 5.0, "Technical Manual," Wolfram Research, Inc.